# Enhancing thermoelectric performance across the electronic phase transition in $Yb_{0.3}Co_4Sb_{12}$

Hong-Jie Pang,[1,2] Hao Yu,[3] Lan Yu,[1] Feng-Xian Bai,[1] Wei-Jian Li,[4,1] Liu-Cheng Chen,[3] Peng-Fei Qiu,[5] Qing Peng,[3,6] and Xiao-Jia Chen[7,*]

[1]*Center for High Pressure Science and Technology Advanced Research, Shanghai 201203, China*

[2]*Key Laboratory of Artificial Structures and Quantum Control (Ministry of Education), School of Physics and Astronomy, Shanghai Jiao Tong University, Shanghai 200240, China*

[3]*School of Science, Harbin Institute of Technology, Shenzhen 518055, China*

[4]*National Laboratory of Solid State Microstructures and School of Physics, Nanjing University, Nanjing 210093, China*

[5]*State Key Laboratory of High Performance Ceramics and Superfine Microstructure, Shanghai Institute of Ceramics, Chinese Academy of Sciences, Shanghai 200050, China*

[6]*State Key Laboratory of Nonlinear Mechanics, Institute of Mechanics, Chinese Academy of Sciences, Beijing 100190, China*

[7]*Department of Physics and Texas Center for Superconductivity, University of Houston, Houston, Texas 77204, USA*

(Received 29 June 2024; revised 6 June 2025; accepted 10 June 2025; published 23 June 2025)

Thermoelectric materials are considered as promising candidates for sustainable energy generation owing to their inherent capability of directly converting waste heat into electricity. Enhancing the thermoelectric conversion efficiency is crucial for their practical applications. Here, we study the pressure effect on the thermoelectric performance in Yb-filled $CoSb_3$ skutterudite, a highly efficient thermoelectric material. By applying external pressure, we find the significant increase of power factor to a high value of 2.9 mW m$^{-1}$ K$^{-2}$ at room temperature. Such an enhancement is attributed to a pressure-driven electronic phase transition, as supported from the electrical transport measurements and electronic band structure calculations. This study thus establishes a connection between thermoelectric performance and the electronic phase transition and points to a route to further increase the power factor through the introduction of the electronic phase transition in thermoelectrics.

DOI: 10.1103/dnjt-81f6

## I. INTRODUCTION

Thermoelectric materials have attracted much attention for sustainable energy applications due to their ability to directly convert waste heat into useful electricity. The conversion efficiency is determined by the dimensionless figure of merit, defined as $zT = S^2\sigma T/\kappa$, where $S$ is the Seebeck coefficient, $\sigma$ is the electrical conductivity, $T$ is the absolute temperature, and $\kappa$ is the thermal conductivity consisting of lattice thermal conductivity ($\kappa_l$) and electronic thermal conductivity ($\kappa_e$) [1]. High performance thermoelectric materials should have high power factor (PF $= S^2\sigma$) and low lattice thermal conductivity [1–5]. Due to the Seebeck coefficient, electrical conductivity and electronic thermal conductivity are interdependent, and extensive efforts concentrate on decoupling or synergistically controlling these parameters to improve the thermoelectric performance. Currently, the typical approaches to improve the thermoelectric performance are band engineering and nanostructuring [3,6,7]. The mechanism of band engineering to enhance thermoelectric performance involves tailoring the electronic band structure of materials, such as manipulating the density of states and optimizing the electronic transport properties, to maximize the Seebeck coefficient, minimize thermal conductivity, and improve the overall thermoelectric efficiency [7]. Nanostructuring involves creating nanoscale structures or interfaces in materials, which introduces phonon scattering and leads to a reduction in thermal conductivity, while maintaining electronic transport properties, resulting in an increased $zT$ for improved thermoelectric efficiency [3]. By utilizing these methods, significant improvements in the performance of thermoelectric materials have been achieved, such as PbTe, SnSe, $Cu_2Se$, and $Bi_2Te_3$ [4,6–10]. Continued research and innovation in this field are expected to unveil more high-efficiency thermoelectric materials in the future.

A "phonon-glass-electron-crystal" material usually has electronic properties typically related to a good semiconductor single crystal and also possesses thermal properties similar to that of an amorphous material, which is thus an ideal candidate for thermoelectric applications [2]. As one striking example of the phonon-glass-electron-crystal concept [2], filled skutterudite compounds have been considered as ideal candidates for thermoelectric materials. The skutterudite structure belongs to the space group $Im\bar{3}$ and consists of corner-shared $MX_6$ octahedra ($M$ = transition metal and $X$ = pnictogen) [11], leaving a void at the body centered site of the cubic unit cell. Such a void could accommodate a foreign atom to form a filled skutterudite with the general formula $R_yM_4X_{12}$ [12], where $R$ is the filled atom and $y$ is the filling fraction. Filling the voids with atoms largely reduces the lattice thermal conductivity without deteriorating the electrical properties [13–19]. Moreover, it is generally believed that the smaller and the heavier the filled atom, the lower the lattice thermal conductivity. Therefore, filling the smaller and

*Contact author: xjchen@uh.edu

 

heavier atom Yb has produced a series of high figure of merits, such as $zT = 1.5$ at 850 K for $Yb_{0.3}Co_4Sb_{12}$ [20], $zT = 1.4$ at 823 K for $Yb_{0.35}Co_4Sb_{12}$ [17], and $zT = 1.4 - 1.7$ for multifilled $Ba_uLa_vYb_wCo_4Sb_{12}$ [21,22]. Additionally, band engineering strategies involve modifying the electronic structure of filled skutterudites through techniques such as doping, alloying, and defect engineering. Nanotechnology approaches focus on synthesizing filled skutterudite nanoparticles and utilizing them in nanocomposite materials to exploit their unique size-dependent properties ($zT = 1.43$ at 800 K) [23]. However, further research and exploration are still needed to unlock the full potential of thermoelectric materials and achieve even higher $zT$ values. Compared with doping and alloying, pressure is recognized as a clean and more effective way to tune the electronic and lattice structure [24–27]. Among filled skutterudites, Yb-filled $CoSb_3$ is one of the most efficient thermoelectric materials [28]. In addition to its low lattice thermal conductivity [29,30], its good electrical transport properties are believed to be attributed to its high carrier mobility, triply degenerate conduction band minimum, and the possible existence of additional electron pockets around the conduction band minimum [2,31–37]. Theoretical calculations have found that in the pristine $CoSb_3$ skutterudite, the band-gap dependence on pressure exhibits a parabolic shape, resulting in a high Seebeck coefficient and power factor [38]. A sudden increase in the Seebeck coefficient with pressure has also been observed in the pristine $CoSb_3$ skutterudite [39]. However, there have been no reports on the electronic structure and thermoelectric properties of Yb-filled $CoSb_3$ skutterudite under pressure.

In this work, we take Yb-filled $CoSb_3$ skutterudite as an example to study the effect of pressure on the electrical transport properties of Yb-filled $CoSb_3$ skutterudite through high-pressure electrical transport measurements and first-principles calculations. The evolution path of the Seebeck coefficient, electrical conductivity, carrier concentration, and effective mass with pressure is investigated in detail. The band structures of Yb-filled skutterudite at various pressures are calculated and analyzed. The results suggest that the electronic phase transition is a powerful means to further improve the thermoelectric performance of highly efficient thermoelectric materials.

## II. EXPERIMENTAL AND CALCULATION DETAILS

The sample was prepared by a melt spinning and spark plasma sintering process. Detailed information is available elsewhere [19,40]. The structure of the sample is characterized by a RigakuD/MAX-2550PC diffractometer under Cu-K$\alpha$ radiation with a wavelength of 1.5406 Å (Fig. S1 in Supplemental Material [40]). The actual composition of the sample is $Yb_{0.3}Co_4Sb_{12}$, which was confirmed by an energy dispersive spectrometer (Oxford Instruments) (Fig. S2 in Supplemental Material [40]).

High-pressure Seebeck coefficient measurements were based on the definition $S = \Delta V/\Delta T$, where $\Delta V$ is the thermopower and $\Delta T$ is the temperature gradient. A symmetric diamond anvil cell was used to provide pressure. The anvil culet was 500 μm in diameter and NaCl was used as the pressure-transmitting medium. A point heat source was utilized as the heat source. The temperature gradient and potential difference between the hot and cold ends were collected by a $T$-type thermocouple and a digital nanovolt meter (218-A5900, Keithley), respectively. The Seebeck coefficient was obtained by fitting the slope of $\Delta V/\Delta T$.

High-pressure resistivity and Hall effect measurements were performed via a physical property measurement system (PPMS) from Quantum Design. A nonmagnetic diamond anvil cell made of Be-Cu alloy was used to provide the pressure environment. The anvil culet was 500 μm in diameter and neon was used as the pressure-transmitting medium. Four platinum electrodes were attached to the four corners of the sample with silver epoxy conductive adhesive. The van der Pauw method was employed to determine the resistivity and Hall coefficient [41]. For all the experiments, the pressure level up to approximately 10 GPa was determined by the standard ruby fluorescent technique [42].

The first-principles calculations were performed on the basis of the density functional theory (DFT) and projector augmented wave method with a Perdew-Burke-Ernzerbof-type generalized gradient approximation, implemented in the Vienna Ab initio Simulation Package [43–45]. All the atomic positions were relaxed to obtain the stable structure. All the lattice parameters as well as internal atomic positions are relaxed with an energy convergence of $10^8$ eV. The wave functions were expanded in the plane waves basis with an energy cutoff of 520 eV. The sampling of the Brillouin zone was done using a Γ-centered $3 \times 3 \times 3$ Monkhorst-Pack grid. All calculations for Yb-filled $CoSb_3$ were performed in a $3 \times 3 \times 1$ supercell (61 atoms, one Yb atom, and a $Co_{12}Sb_{48}$ supercell, corresponding to $Yb_{1/3}Co_4Sb_{12}$). The spin-orbit coupling was included in our calculations.

## III. RESULTS AND DISCUSSION

### A. Pressure dependence of the Seebeck coefficient

The measurement of thermoelectric properties under pressure, especially for the Seebeck coefficient, has been widely accepted in our previous studies [46–48]. Figure 1 illustrates the evolution of the Seebeck coefficient of Yb-filled $CoSb_3$ skutterudite with pressure at 300 K. The cyan sphere represents the result measured at ambient pressure. Within the studied pressure range, the Seebeck coefficient remains negative, indicating electron doping resulting from Yb filling. As the pressure increases, the absolute value of the Seebeck coefficient shows a sudden increase, reaching a maximum value at around 2–3 GPa, and then keeps nearly stable. With a further increase beyond 6 GPa, the absolute value of the Seebeck coefficient exhibits a gradual decrease.

Our previous studies have shown that the Yb-filled skutterudite is stable before 12.4 GPa through high-pressure x-ray diffraction and Raman scattering measurements [29]. Therefore, the significant increase in the absolute value of the Seebeck coefficient around 2–3 GPa is not attributed to a structural phase transition. The sharp change in the Seebeck coefficient is most likely due to the pressure-induced modifications in the electronic structure.

The Boltzmann transport theory offers a comprehensive insight into the Seebeck coefficient, as expressed in the Mott

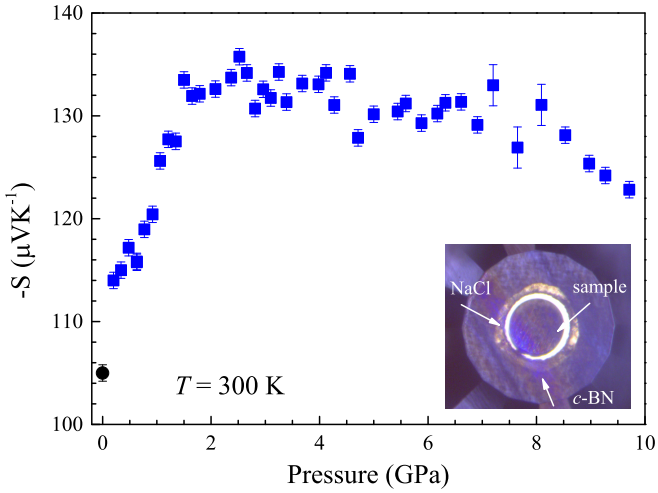


FIG. 1. Pressure dependence of the Seebeck coefficient (S) for $Yb_{0.3}Co_4Sb_{12}$ at 300 K. The inset shows the diagram of Seebeck coefficient measurements under pressure. The sample is placed in the chamber, which is surrounded by cubic boron nitride as insulating layers. NaCl is used as the pressure-transmitting medium. The cyan sphere represents the data measured from the PPMS at ambient pressure. The error bars correspond to the uncertainties of the measured data.

equation [49–52]:

$$S = \frac{\pi^2}{3}\frac{k_B}{e}k_BT\left\{\frac{d\{ln[\sigma(E)]\}}{dE}\right\}_{E=E_F} = \frac{\pi^2}{3}\frac{k_B}{e}k_BT\left\{\frac{1}{n}\frac{dn(E)}{dE}+\frac{1}{\mu}\frac{d\mu(E)}{dE}\right\}_{E=E_F}, \quad (1)$$

where $e$ is the carrier charge, $k_B$ is the Boltzmann constant, $n(E)$ is the energy-dependent carrier concentration, and $\mu(E)$ is the energy-dependent carrier mobility. Additionally, $\sigma(E)$ corresponds to the electrical conductivity determined based on band filling or Fermi energy level denoted as $E_F$. The expression for electrical conductivity is $\sigma(E) = n(E)e\mu(E)$, where the carrier concentration $n(E) = g(E)f(E)$, $g(E)$ is the state density, and $f(E)$ is the Fermi function.

The Seebeck coefficient in the Mott equation serves as a measure of the variation in $\sigma(E)$ near the Fermi level. This variation is reflected in the logarithmic derivative of $\sigma$ with $E$. Consequently, the Seebeck coefficient characterizes the asymmetry in electronic structure and scattering rates in the vicinity of the Fermi level. In order to achieve a large Seebeck coefficient, it is crucial to introduce complexities in the electronic structure and scattering rates within a narrow energy range (a few $k_BT$) near $E_F$. When electronic scattering is energy independent, the $\sigma(E)$ is directly related to the density of states (DOS) at $E$. A material exhibiting a significant variation in DOS near the Fermi level is anticipated to possess a relatively large Seebeck coefficient.

In degenerate semiconductors, the density of states $g(E)$ can be determined in the context of effective mass $m_d^*$ as [1,7]

$$g(E) = \frac{(m_d^*)^{3/2}\sqrt{2E}}{\hbar^3\pi^2}. \quad (2)$$

The Seebeck coefficient $S$ is thus equivalently expressed based on $m_d^*$ and the carrier concentration $n_H$ as [1,7]

$$S = \frac{8\pi^2k_B^2T}{3qh^2}m_d^*\left(\frac{\pi}{3n_H}\right)^{2/3}. \quad (3)$$

Therefore, several factors can contribute to an increase in the Seebeck coefficient in Yb-filled $CoSb_3$ skutterudite, with the Lifshitz transition and an increase in band gap being the two most probable causes. The asymmetrical change of the Seebeck coefficient under external pressure is a classical characteristic of the Lifshitz transition [53]. The Seebeck coefficient, being the derivative of the Fermi level state density concerning energy, is significantly affected by the topological properties of electrons. The Lifshitz transition can enhance the Seebeck coefficient and electrical conductivity by increasing the number of energy bands near the Fermi surface, thereby increasing the electronic density of states.

Additionally, the Seebeck coefficient is proportional to the band gap according to the Goldsmid-Sharp equation [54]. Hence, an alternative mechanism could be widening of the band gap under pressure, leading to an increased effective mass of the sample. Equation (3) also shows that the Seebeck coefficient is directly linked to the effective mass. As a result, an increase in the band gap could potentially enhance the Seebeck coefficient. The nonmonotonic behavior of the Seebeck coefficient under pressure indicates the involvement of various underlying mechanisms affecting its behavior, highlighting the need for deeper examination and analysis.

### B. High-pressure resistivity and power factor

Changes in the electronic structure of a sample can be reflected in its resistivity, particularly when additional energy bands cross the Fermi level and cause a transition related to van Hove singularities in the DOS. Alterations in the band gap directly affect both effective mass and mobility, which are observable through measured resistivity [55–58]. To investigate possible evidence of electronic structure changes, we performed high-pressure resistivity measurements. Figure 2(a) shows the variation of the resistivity of Yb-filled $CoSb_3$ skutterudite as a function of pressure at 300 K, where the cyan spheres denote the results measured at ambient pressure. With increasing pressure, the resistivity increases significantly, with a notable change in the curvature of the resistivity increase occurring around 3 GPa. As the pressure continues to increase, the resistivity reaches a maximum near 4 GPa. Further increasing the pressure leads to a gradual decrease in the resistivity. Previous investigations have demonstrated the absence of any structural phase transition in the Yb-filled $CoSb_3$ skutterudite within the examined pressure range [29]. Consequently, the abrupt change in resistivity around 3 GPa cannot be attributed to a structural phase transition but may be ascribed to a transition in the electronic structure. The presence of extrema in resistivity also suggests the potential existence of multiple competing mechanisms within the sample.

By combining the Seebeck coefficient and resistivity, we can determine the power factor of Yb-filled $CoSb_3$ skutterudite under varying pressure conditions, as illustrated in Fig. 2(b). The power factor exhibits a significant increase with increasing pressure, reaching its maximum value of

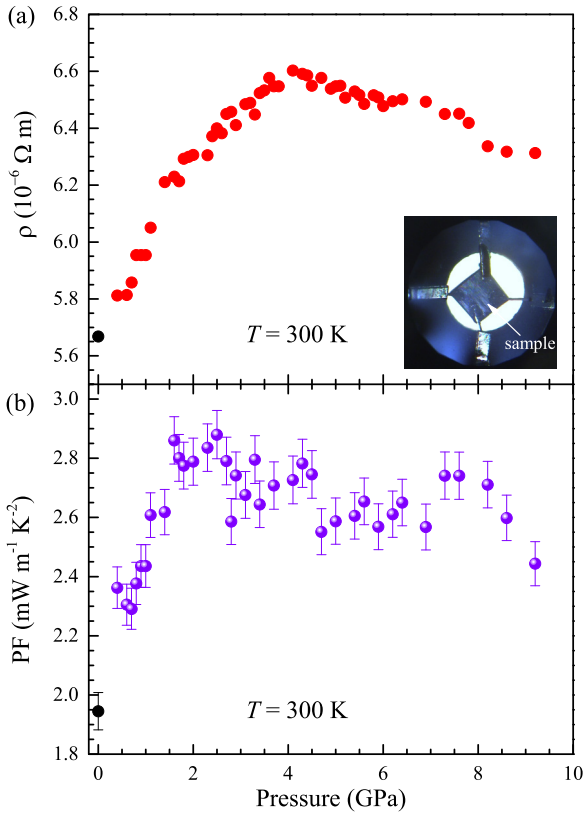


FIG. 2. (a) Pressure dependence of the resistivity ($\rho$) at 300 K. The inset shows the geometry of the electrical transport measurements at 0.7 GPa. The sample is in the middle. Four Pt wires are attached to the sample. (b) Pressure dependence of the power factor (PF) at 300 K. The cyan spheres represent the data measured from the PPMS at ambient pressure. The error bars correspond to the uncertainties of all the related experimental data.

2.9 mW m$^{-1}$ K$^{-2}$ near the critical pressure of approximately 2.5 GPa. Subsequently, as the pressure continues to increase, the power factor remains nearly constant until it experiences a rapid decline beyond 8 GPa. Although the power factor is still relatively low compared to those of many other efficient thermoelectric materials [25–27], we observed a significant improvement upon the application of pressure. Specifically, compared with the power factor of this compound at ambient pressure, the maximum power factor is increased by nearly 50%.

The pressure-induced enhancement of the power factor has also been observed in the parent $CoSb_3$ skutterudite [39]. Researchers employed a novel high-pressure Seebeck coefficient measurement method to evaluate the Seebeck coefficient and resistivity of the $CoSb_3$ skutterudite within a pressure range of 0–25 GPa. The Seebeck coefficient of the $CoSb_3$ skutterudite exhibits a rapid increase with increasing pressure, reaching its maximum value near 10 GPa, followed by a gradual decrease and stabilization. Simultaneously, the resistivity gradually increases under pressure, displaying a change in curvature around 10 GPa. Consequently, the power factor demonstrates a peak value near 10 GPa. The observed trends of the Seebeck coefficient, resistivity, and power factor with pressure in parent $CoSb_3$ are consistent with those observed in Yb-filled $CoSb_3$. The difference is that the pressure point at which the transition occurs is shifted to the lower value due to the filling of Yb atoms.

Typically, pressure regulation of the electrical transport properties in a sample is mainly manifested in its influence on the electronic structure, rather than doping or solid solution, which primarily relies on an increase in carrier concentration by several orders of magnitude. The enhancement of the power factor under pressure may arise from two aspects. First, it can result from reducing the energy differences between multiple band extrema, thereby inducing a Lifshitz transition. Second, it can involve tuning the intrinsic band gap of the sample to align with the most suitable value under the current temperature range ($6\,k_BT < E_g < 10\,k_BT$) [59]. Additionally, there are also special cases to consider, such as triggering anomalous Hall effect, which depend on specific materials. Further examination requires the measurement of additional electrical transport parameters.

### C. Pressure-dependent carrier concentration, mobility, and effective mass

To gain a deeper understanding of the changes in the electronic structure of Yb-filled $CoSb_3$ skutterudite, we conducted high-pressure Hall resistivity measurements. Since the Hall effect near room temperature stems from bulk charge carriers, we employed a single-band model and calculated the carrier concentration, $n_H = 1/(eR_H)$, where $R_H$ is the Hall coefficient. The carrier mobility can be determined from $\mu = \sigma/n_H e$.

The pressure dependence of carrier concentration is shown in Fig. 3(a), where the green circles represent the measurements taken at ambient pressure. At ambient pressure, the carrier concentration of Yb-filled $CoSb_3$ is close to the optimum value, approximately $1 \times 10^{20}$ cm$^{-3}$. With increasing pressure, there is a monotonic increase in the carrier concentration, and a change in curvature occurs around 3 GPa. As pressure continues to increase, the carrier concentration stabilizes at around $8 \times 10^{20}$ cm$^{-3}$ after reaching 6 GPa. The trend of carrier mobility, as depicted in Fig. 3(b), exhibits an inverse relationship with carrier concentration. With increasing pressure, the mobility gradually diminishes, undergoes a change in curvature around 3 GPa, and eventually stabilizes beyond 6 GPa.

Figure 3(c) shows the Seebeck effective mass ($m_S^*$) of Yb-filled $CoSb_3$ skutterudite at different pressures, with the green circles representing the measurements taken at ambient pressure. For thermoelectric materials, the effective mass is synonymous with the Seebeck effective mass. The Seebeck effective mass can be calculated using the experimentally measured Seebeck coefficient and the carrier concentration obtained through the Hall effect through the following formula [60]:

$$\frac{m_S^*}{m_e} = 0.924\left(\frac{300K}{T}\right)\left(\frac{n_H}{10^{20}cm^{-3}}\right)^{2/3} \times \left[\frac{3\left(\exp\left[\frac{|S|}{k_B/e}\right] - 0.17\right)^{2/3}}{1+\exp\left[-5\left(\frac{|S|}{k_B/e} - \frac{k_B/e}{|S|}\right)\right]} + \frac{\frac{|S|}{k_B/e}}{1+\exp\left[5\left(\frac{|S|}{k_B/e} - \frac{k_B/e}{|S|}\right)\right]}\right]. \quad (4)$$

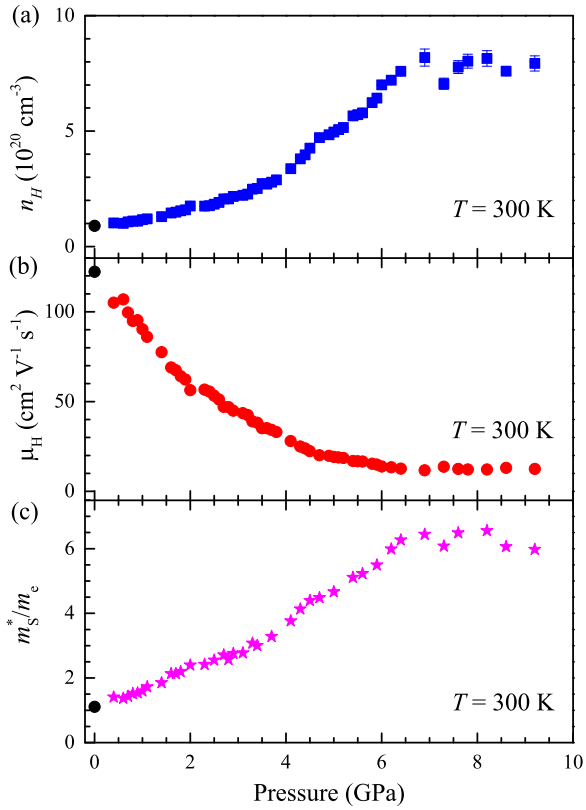


FIG. 3. Pressure dependence of the carrier concentration ($n_H$) (a), the carrier mobility ($\mu_H$) (b), and the normalized Seebeck effective mass ($m_S^*/m_e$) (c) in Yb-filled $CoSb_3$ skutterudite. The cyan spheres correspond to the data at ambient pressure. The error bars correspond to the uncertainties of the measured data. Some error bars cannot be seen because the errors are smaller than the symbol sizes.

The formula can be used to estimate the Seebeck effective mass. When the absolute value of the Seebeck coefficient is greater than 20 $\mu V\,K^{-1}$, the relative error of the results is approximately 3%. The effective mass exhibits a consistent trend with the carrier concentration under varying pressure, as depicted in Fig. 3(c). As the pressure increases, there is a gradual increase in the effective mass, accompanied by a change in curvature around 3 GPa. Subsequently, beyond 6 GPa, the effective mass tends to stabilize.

According to Eq. (4), the enhancement of the single-band effective mass of Yb-filled $CoSb_3$ suggests an increase in the band gap due to the decrease in carrier mobility. However, the significant increase in carrier concentration cannot be solely attributed to the increase in band gap and requires consideration of the possibility of a Lifshitz transition or specific band structures in the sample. This observation is consistent with the observed increase in effective mass. Considering the aforementioned measurement results, we postulate that the notable enhancement in the electrical transport properties arises from a pressure-induced electronic phase transition. Furthermore, it is worth noting that the magnitude of the enhancement in the power factor is also limited by the increase in the band gap. To verify this hypothesis, we conducted band structure calculations under pressure conditions.

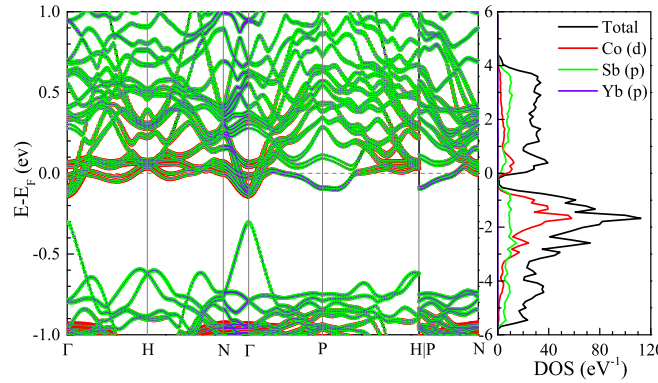


FIG. 4. The band structure and projected density of states for Yb-filled $CoSb_3$ skutterudite.

### D. Pressure evolution of the electronic structure

The parent compound $CoSb_3$ is a direct band-gap semiconductor with unique electronic properties [31–33,37]. It exhibits linear dispersion in both valence and conduction bands near the Fermi surface at the Γ point. The valence bands are primarily occupied by Co-$p/d$ and Sb-$p$ orbital electrons, while the conduction bands consist of Co-$d$ orbital electrons. When Yb is introduced into $CoSb_3$, the electronic band structure remains significantly unchanged, as confirmed by previous calculations [31,33,34,37]. However, the band gap increases with Yb filling [34,37], with DFT calculations yielding values of 0.12 eV for $CoSb_3$ and 0.29 eV for $YbCo_4Sb_{12}$, respectively [32,37,61].

The band structure and projected density of states of $Yb_{0.3}Co_4Sb_{12}$ at ambient pressure are depicted in Fig. 4. The band-gap value along the $\Gamma \rightarrow T$ direction is 0.16 eV (CB1). Moreover, the conduction band bottom has a subband bottom along the $\Gamma \rightarrow N$ direction, corresponding to a band gap value of approximately 0.31 eV (CB2). Particularly, there is another degenerate point of the conduction band bottom along the $\Gamma \rightarrow P$ direction, corresponding to a band gap value of CB3. Compared to $CoSb_3$, the band gap along the $\Gamma \rightarrow P$ direction in Yb-filled $CoSb_3$ skutterudite is reduced, possibly due to changes in bond length or orbital hybridization induced by the filling atoms. It is worth noting that the band gap along the $\Gamma \rightarrow P$ direction is comparable to that along the $\Gamma \rightarrow N$ direction in the Yb-filled $CoSb_3$ skutterudite. The calculated results are consistent with those in the literature [62].

To investigate the pressure-induced variation of the band gap, we extracted the band gaps CB1, CB2, and CB3 along the Γ point and $\Gamma \rightarrow N$ and $\Gamma \rightarrow P$ directions at different pressures (Fig. 5). It is evident that within the studied pressure range, the band gap of Yb-filled $CoSb_3$ skutterudite gradually increases with increasing pressure. Moreover, the differences in band gaps along these directions decrease and tend to converge. The observed dependence of band gap on pressure exhibits a parabolic trend consistent with previous studies on parent $CoSb_3$ skutterudite's response to pressure variations [38]. This characteristic holds promise for achieving an exceptionally high Seebeck coefficient and outstanding thermoelectric performance.

It is worth noting that a transition from a direct band-gap semiconductor to an indirect band-gap semiconductor occurs

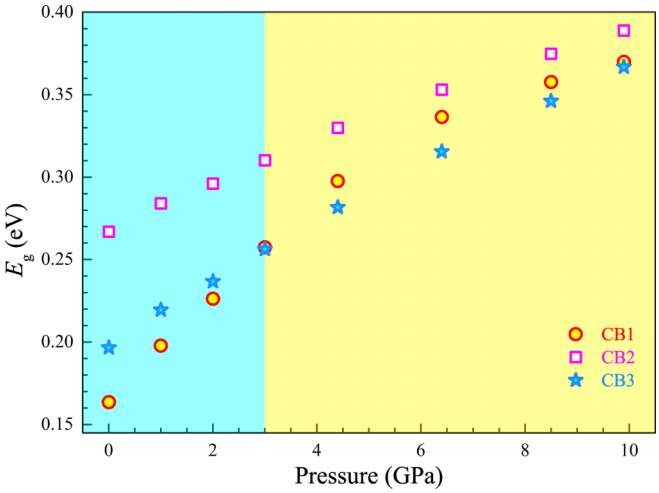


FIG. 5. Evolution of the band gap near the Γ high-symmetry point with pressure. CB1, CB2, and CB3 denote the band gap along the direction of $\Gamma \rightarrow T$, $\Gamma \rightarrow N$, and $\Gamma \rightarrow P$, respectively.

when the pressure exceeds 3 GPa. With increasing pressure, the conduction band reaches its minimum energy point at the Γ point and converges along the $\Gamma \rightarrow P$ direction around 3 GPa. As the pressure continues to increase, the Yb-filled $CoSb_3$ skutterudite changes its band gap from direct to indirect. This observation is consistent with previous findings on the parent $CoSb_3$ skutterudite [38,39], suggesting an occurrence of electronic phase transition in Yb-filled $CoSb_3$ skutterudite at approximately 3 GPa, which precedes that of $CoSb_3$ (6 GPa).

Within the entire pressure range, the top of the valence band at the Γ point shows little change relative to the Fermi surface. In contrast, the bottom of the conduction band at the Γ point moves upward, resulting in an increase in the band gap. This is similar to the reported results in the parent compound $CoSb_3$ [38].

As mentioned earlier, with increasing pressure, the hybridization between the valence and conduction bands of the filled skutterudite increases, leading to a decrease in the indirect band gap and an increase in the direct band gap. Usually, when the band gap closes, both the resistivity and Seebeck coefficient significantly decrease with increasing pressure. The competition between these two factors during the closure of the band gap can have a substantial impact on the power factor. In the case of Yb-filled $CoSb_3$ skutterudite, the band gap increases with increasing pressure. Therefore, the Seebeck coefficient and resistivity also increase with increasing pressure.

### E. Pressure-driven electronic phase transition

The band structure calculations reveal an electronic phase transition occurring around 3 GPa in Yb-filled $CoSb_3$ skutterudite. This finding is consistent with the anomalous observations in electrical transport measurements within the pressure range of 3–4 GPa, suggesting that the enhancement of the power factor arises as a consequence of the electronic phase transition. As the band structure gradually converges under increasing pressure and approaches energy degeneracy, there is an increased energy dependence and peak density of states near the Fermi surface around the electronic phase transition (Fig. 4). This can be attributed to the localization process of high-density states at smaller energy ranges during the convergence of valence band bottom energies at Γ and $P$ points, ultimately leading to complete localization at a specific energy upon degeneracy.

Following Eq. (1), one learns that an increase in the density of states due to the band convergence contributes positively to the Seebeck coefficient. Considering the significant difference in carrier mobility between the linear bands at the Γ point and the parabolic bands at the $P$ point, one can find an enhancement during the band convergence process. As a result, the Seebeck coefficient increases accordingly. The subsequent decrease is primarily due to the dominant effect of increased carrier concentration, consistent with the decrease in resistivity during this stage.

Before the electronic phase transition, the increase in carrier concentration mainly relies on the density of states at the Γ point, which increases slowly. After the electronic phase transition, the energy bands at the Γ and $P$ points become degenerate, resulting in an increased density of states and an accelerated increase in carrier concentration.

In addition to the aforementioned changes, we also observed an increase in the band gap during the compression process, which is consistent with the decreased carrier mobility and corresponds to an increase in the effective mass of the single band. Before the electronic phase transition, the increase in carrier concentration increases slowly, and the dominant factor is the increase in effective mass caused by the increased band gap. Consequently, the resistivity gradually decreases. The overall improvement in the power factor of the sample is influenced not only by the increase in carrier concentration and electronic phase transition but also by the modulation of the increased band gap. Before the electronic phase transition, although the increase in the band gap contributes positively to the Seebeck coefficient, it has a relatively strong inhibitory effect on the resistivity. In the context of the single-band model, for the sample to exhibit the optimal power factor at room temperature, the band gap should ideally range between 0.15 and 0.25 eV. A deviation from this range hinders the achievement of the optimal power factor. Therefore, the increase in band gap to some extent restricts the improvement in the power factor of Yb-filled $CoSb_3$ skutterudites through the electronic phase transition at room temperature. However, Yb-filled $CoSb_3$ skutterudites still achieve a ≈50% improvement under pressure. If the increase in the band gap can be suppressed, it may further enhance the thermoelectric performance of the sample at room temperature. Meanwhile, the increase in the band gap favors the shift of the optimal operating temperature range of the sample towards higher temperatures, making the Yb-filled $CoSb_3$ skutterudites under pressure more suitable for thermoelectric applications at higher temperature regions.

### F. Thermoelectric measure for electronic phase transition

As an electronic phase transition characterized by the absence of Landau-type order parameters and symmetry breaking, the Lifshitz transition was proposed by Lifshitz in the 1960s [53]. The distinguishing feature of a Lifshitz transition

lies in the topological modification of Fermi surfaces induced by external parameters. The Lifshitz transition can initially be identified, such as the emergence of superconductivity in simple metals [63]. Moreover, Lifshitz transitions play a key role in strongly correlated systems, including high-temperature superconductors and heavy-fermion itinerant magnets [58,64–67]. However, these systems were usually characterized by strong coupling between different degrees of freedom, and the significance of the Lifshitz transition becomes obscured. Furthermore, the inherent difficulties in directly observing the Fermi surface in strongly correlated systems make it nearly impossible to detect Lifshitz transitions directly.

The Lifshitz transition, characterized by changes in Fermi surface shape and accompanied by singularities in thermodynamic and dynamical features, can be measured through thermopower according to Abrikosov's suggestion in his work [68–70]. Applying pressure is the most suitable and clean method for achieving Lifshitz transitions, as it allows continuous tuning without introducing defects or impurity. Compared to compositional tuning, pressure-driven transitions offer a relatively wide range of lattice deformation and are more effective in studying pure intrinsic properties [24,63,71]. Near the Lifshitz transition or in the vicinity of singular points, the Seebeck coefficient can exhibit asymmetric behavior due to its dependence on different sides of the Fermi surface with respect to the chemical potential, potentially leading to a change in sign [55,71]. Thus, observing whether the Seebeck coefficient changes sign or exhibits asymmetric shape around the Lifshitz transition, particularly under pressure, serves as the most direct and reliable approach for identifying and determining the occurrence of this transition.

In the initial investigations, Lifshitz [53] examined the singularities that arise in proximity to the Lifshitz transition and proposed the necessity of integrating thermodynamic and dynamic quantities, such as thermal expansion, sound velocity, electrical conductivity, and thermal conductivity, for detecting this transition due to their manifestation of singularity near the critical point. Subsequent theoretical [71,72] and experimental studies [73] have revealed that the electrical conductivity, similar to the Seebeck coefficient, exhibits significant deviations near the transition point, deviating from the continuous behavior typically observed under external influences and displaying changes in curvature.

In addition to alterations in electronic characterization-related physical properties, it is anticipated that various physical quantities reflecting lattice dynamics, such as sound velocity [53], thermal expansion [53,72], and thermal conductivity [53], will manifest anomalous behaviors in proximity to the Lifshitz transition. Thermal conductivity is a fundamental physical parameter that characterizes the ability of a material to transport heat, encompassing both lattice and electronic contributions. The electronic thermal conductivity can be expressed as $\kappa_e = L\sigma T$, where $L$ is the Lorenz number. Conversely, the lattice thermal conductivity is directly influenced by the group velocity of phonons. Due to significant deviations from the regular trend near the Lifshitz transition, the electrical conductivity exhibits notable changes in curvature. Consequently, both electronic and lattice thermal conductivities display abrupt behavior, leading to pronounced alterations in the total thermal conductivity near the Lifshitz transition. By investigating the variations in thermal conductivity, we can not only unveil the expected anomalous contributions of lattice dynamics near the Lifshitz transition but also capture the abrupt changes in anticipated electrical conductivity at this critical point. It is evident that thermal conductivity, as a thermodynamic parameter, is poised to exhibit significant anomalies in proximity to Lifshitz transitions. Recent experimental studies have indeed demonstrated that exploring the evolution of thermoelectric behavior under pressure serves as an effective approach to help identify Lifshitz transitions [25–27]. While the precise determination of Fermi surface topology in $Yb_{0.3}Co_4Sb_{12}$ presents significant computational challenges, direct experimental verification of its evolution under pressure remains absent within the scope of this work. These limitations preclude definitive confirmation of a Lifshitz transition. However, the observed anomalies in transport properties and band structure evolution collectively provide compelling indirect evidence, highlighting the need for advanced characterization techniques to resolve the underlying electronic mechanisms.

Lifshitz transitions mostly remain at the theoretical level and are difficult to observe experimentally. As we have summarized, measuring the Seebeck coefficient, electrical conductivity, and thermal conductivity, and consequently their unified quantity, the thermoelectric figure of merit, is the means to infer whether Lifshitz transition occurs. Therefore, the thermoelectric figure of merit $zT$ is expected to clarify the pure effects of Lifshitz transitions.

## IV. CONCLUSIONS

In summary, we have investigated the influence of pressure on the electronic properties of Yb-filled $CoSb_3$ skutterudites by employing the combined electrical transport measurements and first-principles calculations. By manipulating external pressure, we found a significant enhancement of the power factor at room temperature at pressure of approximately 3 GPa. The electronic phase transition has been identified through abrupt changes observed in the Seebeck coefficient, resistivity, carrier concentration, and band gap. The thermoelectric improvement can be attributed to the electronic phase transition phenomenon. Furthermore, we proposed to utilize thermoelectric performance as a means to help identify the occurrence of the electronic phase transition in thermoelectric materials or similar narrow band-gap semiconductors or semimetals.

## ACKNOWLEDGMENTS

We thank Professor X. Shi and Professor L. D. Chen for providing samples and valuable discussions. We are grateful for the helpful guidance from Professor Xiao-Qun Wang from Shanghai Jiaotong University. This work is funded through the Shenzhen Science and Technology Program (Grant No. KQTD20200820113045081) and the Basic Research Program of Shenzhen (Grant No. JCYJ20200109112810241).

## DATA AVAILABILITY

The data that support the findings of this study are available from the corresponding author upon reasonable request.

[1] G. J. Snyder and E. S. Toberer, Complex thermoelectric materials, Nat. Mater. **7**, 105 (2008).

[2] G. A. Slack, *CRC Handbook of Thermoelectrics*, edited by D. M. Rowe (CRC, Boca Raton, FL, 1995).

[3] B. Poudel, Q. Hao, Y. Ma, Y. C. Lan, A. Minnich, B. Yu, X. Yan, D. Z. Wang, A. Muto, D. Vashaee, X. Y. Chen, J. M. Liu, M. S. Dresselhaus, G. Chen, and Z. F. Ren, High-thermoelectric performance of nanostructured bismuth antimony telluride bulk alloys, Science **320**, 634 (2008).

[4] K. Biswas, J. Q. He, I. D. Blum, C. I. Wu, T. P. Hogan, D. N. Seidman, V. P. Dravid, and M. G. Kanatzidis, High-performance bulk thermoelectrics with all-scale hierarchical architectures, Nature (London) **489**, 414 (2012).

[5] J. Ma, O. Delaire, A. F. May, C. E. Carlton, M. A. McGuire, L. H. VanBebber, D. L. Abernathy, G. Ehlers, T. Hong, A. Huq, W. Tian, V. M. Keppens, Y. Shao-Horn, and B. C. Sales, Glass-like phonon scattering from a spontaneous nanostructure in $AgSbTe_2$, Nat. Nanotechnol. **8**, 445 (2013).

[6] Y. Z. Pei, X. Y. Shi, A. LaLonde, H. Wang, L. D. Chen, and G. J. Snyder, Convergence of electronic bands for high performance bulk thermoelectrics, Nature (London) **473**, 66 (2011).

[7] J. P. Heremans, V. Jovovic, E. S. Toberer, A. Saramat, K. Kurosaki, A. Charoenphakdee, S. Yamanaka, and G. J. Snyder, Enhancement of thermoelectric efficiency in PbTe by distortion of the electronic density of states, Science **321**, 554 (2008).

[8] H. L. Liu, X. Shi, F. F. Xu, L. L. Zhang, W. Q. Zhang, L. D. Chen, Q. Li, C. Uher, T. Day, and G. J. Snyder, Copper ion liquid-like thermoelectrics, Nat. Mater. **11**, 422 (2012).

[9] L. D. Zhao, S. H. Lo, Y. S. Zhang, H. Sun, G. J. Tan, C. Uher, C. Wolverton, V. P. Dravid, and M. G. Kanatzidis, Ultralow thermal conductivity and high thermoelectric figure of merit in SnSe crystals, Nature (London) **508**, 373 (2014).

[10] Y. Pan, U. Aydemir, J. A. Grovogui, I. T. Witting, R. Hanus, Y. B. Xu, J. S. Wu, C.-F. Wu, F.-H. Sun, H.-L. Zhuang, J.-F. Dong, J.-F. Li, V. P. Dravid, and G. J. Snyder, Melt-centrifuged $(Bi, Sb)_2Te_3$: Engineering microstructure toward high thermoelectric efficiency, Adv. Mater. **30**, 1802016 (2018).

[11] B. C. Sales, D. Mandrus, and R. K. Williams, Filled skutterudite antimonides: A new class of thermoelectric materials, Science **272**, 1325 (1996).

[12] T. Schmidt, G. Kliche, and H. D. Lutz, $CoSb_3$, Structure refinement of skutterudite-type cobalt triantimonide, Acta Cryst. C **43**, 1678 (1987).

[13] D. T. Morelli, G. P. Meisner, B. X. Chen, S. Q. Hu, and C. Uher, Cerium filled and doping of cobalt triantimonide, Phys. Rev. B **56**, 7376 (1997).

[14] X. Shi, H. Kong, C.-P. Li, C. Uher, J. Yang, J. R. Salvador, H. Wang, L. Chen, and W. Zhang, Low thermal conductivity and high thermoelectric figure of merit in *n*-type $Ba_xYb_yCo_4Sb_{12}$ double-filled skutterudites, Appl. Phys. Lett. **92**, 182101 (2008).

[15] Y. Z. Pei, J. Yang, L. D. Chen, W. Zhang, J. R. Salvador, and J. H. Yang, Improving thermoelectric performance of caged compounds through light-element filling, Appl. Phys. Lett. **95**, 042101 (2009).

[16] H. Li, X. F. Tang, X. L. Su, Q. J. Zhang, and C. Uher, Nanostructured bulk $Yb_xCo_4Sb_{12}$ with high thermoelectric performance prepared by the rapid solidification method, J. Phys. D **42**, 145409 (2009).

[17] T. Dahal, Q. Jie, G. Joshi, S. Chen, C. F. Guo, Y. C. Lan, and Z. F. Ren, Thermoelectric property enhancement in Yb-doped *n*-type skutterudites $Yb_xCo_4Sb_{12}$, Acta Mater. **75**, 316 (2014).

[18] Y. L. Tang, R. Hanus, S. W. Chen, and G. J. Snyder, Solubility design leading to high figure of merit in low-cost Ce-$CoSb_3$ skutterudites, Nat. Commun. **6**, 7584 (2015).

[19] Y. L. Li, P. F. Qiu, Z. Xiong, J. K. Chen, R. Nunna, X. Shi, and L. D. Chen, Electrical and thermal transport properties of $Yb_xCo_4Sb_{12}$ filled skutterudites with ultrahigh carrier concentrations, AIP Adv. **5**, 117239 (2015).

[20] S. Y. Wang, J. R. Salvador, J. Yang, P. Wei, B. Duan, and J. H. Yang, High-performance *n*-type $Yb_xCo_4Sb_{12}$: From partially filled skutterudites towards composite thermoelectrics, NPG Asia Mater. **8**, e285 (2016).

[21] X. Shi, J. Yang, J. R. Salvador, M. F. Chi, J. Y. Cho, H. Wang, S. Q. Bai, J. H. Yang, W. Q. Zhang, and L. D. Chen, Multiple-filled skutterudites: High thermoelectric figure of merit through separately optimizing electrical and thermal transports, J. Am. Chem. Soc. **133**, 7837 (2011).

[22] X. Shi, S. Q. Bai, L. L. Xi, J. Yang, W. Q. Zhang, L. D. Chen, and J. H. Yang, Realization of high thermoelectric performance in *n*-type partially filled skutterudites, J. Mater. Res. **26**, 1745 (2011).

[23] H. Li, X. F. Tang, Q. J. Zhang, and C. Uher, High performance $In_xCe_yCo_4Sb_{12}$ thermoelectric materials with in situ forming nanostructured InSb phase, Appl. Phys. Lett. **94**, 102114 (2009).

[24] H. K. Mao, X. J. Chen, Y. Ding, B. Li, and L. Wang, Solids, liquids, and gases under high pressure, Rev. Mod. Phys. **90**, 015007 (2018).

[25] L. C. Chen, P. Q. Chen, W. J. Li, Q. Zhang, V. V. Struzhkin, A. F. Goncharov, Z. F. Ren, and X. J. Chen, Enhancement of thermoelectric performance across the topological phase transition in dense lead selenide, Nat. Mater. **18**, 1321 (2019).

[26] T. Nishimura, H. Sakai, H. Mori, K. Akiba, H. Usui, M. Ochi, K. Kuroki, A. Miyake, M. Tokunaga, Y. Uwatoko, K. Katayama, H. Murakawa, and N. Hanasaki, Large enhancement of thermoelectric efficiency due to a pressure-induced Lifshitz transition in SnSe, Phys. Rev. Lett. **122**, 226601 (2019).

[27] F. X. Bai, H. Yu, Y. K. Peng, S. Li, L. Yin, G. Huang, L. C. Chen, A. F. Goncharov, J. H. Sui, F. Cao, J. Mao, Q. Zhang, and X. J. Chen, Electronic topological transition as a route to improve thermoelectric performance in $Bi_{0.5}Sb_{1.5}Te_3$, Adv. Sci. **9**, 2105709 (2022).

[28] G. S. Nolas, D. T. Morelli, and T. M. Tritt, Skutterudites: A phonon-glass-electron-crystal approach to advanced thermoelectric energy conversion applications, Annu. Rev. Mater. Res. **29**, 89 (1999).

[29] H. J. Pang, L. C. Chen, H. Yu, P. F. Qiu, G. H. Zhong, Q. Peng, and X. J. Chen, Hybridization-driven strong anharmonicity in Yb-filled skutterudites, Phys. Rev. B **105**, 094115 (2022).

[30] H. J. Pang, H. Yu, W. J. Li, L. C. Chen, P. F. Qiu, Q. Peng, and X. J. Chen, High-order phonon anharmonicity in Yb-filled skutterudites, Phys. Rev. B **109**, 045201 (2024).

[31] D. J. Singh and W. E. Pickett, Skutterudite antimonides: Quasilinear bands and unusual transport, Phys. Rev. B **50**, 11235 (1994).

[32] J. O. Sofo and G. D. Mahan, Electronic structure of $CoSb_3$: A narrow-band-gap semiconductor, Phys. Rev. B **58**, 15620 (1998).

[33] Y. L. Tang, Z. M. Gibbs, L. A. Agapito, G. D. Li, H. S. Kim, M. B. Nardelli, S. Curtarolo, and G. J. Snyder, Convergence of multi-valley bands as the electronic origin of high thermoelectric performance in $CoSb_3$ skutterudites, Nat. Mater. **14**, 1223 (2015).

[34] E. B. Isaacs and C. Wolverton, Electronic structure and phase stability of Yb-filled $CoSb_3$ skutterudite thermoelectrics from first-principles, Chem. Mater. **31**, 6154 (2019).

[35] J. C. Smith, S. Banerjee, V. Pardo, and W. E. Pickett, Dirac point degenerate with massive bands at a topological quantum critical point, Phys. Rev. Lett. **106**, 056401 (2011).

[36] V. Pardo, J. C. Smith, and W. E. Pickett, Linear bands, zero-momentum Weyl semimetal, and topological transition in skutterudite-structure pnictides, Phys. Rev. B **85**, 214531 (2012).

[37] H. J. Pang, H. Yu, W. J. Li, L. C. Chen, P. F. Qiu, Q. Peng, and X. J. Chen, Topological states of thermoelectric Yb-filled skutterudites, Phys. Rev. B **107**, 125202 (2023).

[38] X. X. Yang, Z. H. Dai, Y. C. Zhao, W. C. Niu, J. Y. Liu, and S. Meng, Pressure induced excellent thermoelectric behavior in skutterudites $CoSb_3$ and $IrSb_3$, Phys. Chem. Chem. Phys. **21**, 851 (2019).

[39] L. Wu, Y. Sun, G. Z. Zhang, and C. X. Gao, Pressure-induced improvement of Seebeck coefficient and thermoelectric efficiency of $CoSb_3$, Mater. Lett. **129**, 68 (2014).

[40] See Supplemental Material at http://link.aps.org/supplemental/10.1103/dnjt-81f6 for the details of the quality of the sample.

[41] L. J. van der Pauw, A method of measuring specific resistivity and Hall effect of discs of arbitrary shape, Philips Res. Repts. **13**, 1 (1958).

[42] H. K. Mao, P. M. Bell, J. W. Shaner, and D. J. Stembey, Specific volume measurements of Cu, Mo, Pd, and Ag and calibration of the ruby R1 fluorescence pressure gauge from 0.06 to 1 Mbar, J. Appl. Phys. **49**, 3276 (1978).

[43] G. Kresse and D. Joubert, From ultrasoft pseudopotentials to the projector augmented-wave method, Phys. Rev. B **59**, 1758 (1999).

[44] G. Kresse and J. Furthmüller, Efficient iterative schemes for ab initio total-energy calculations using a plane-wave basis set, Phys. Rev. B **54**, 11169 (1996).

[45] J. P. Perdew, K. Burke, and M. Ernzerhof, Generalized gradient approximation made simple, Phys. Rev. Lett. **77**, 3865 (1996).

[46] H. Yu, L. C. Chen, H. J. Pang, X. Y. Qin, P. F. Qiu, X. Shi, L. D. Chen, and X. J. Chen, Impressive enhancement of thermoelectric performance in $CuInTe_2$ upon compression, Mater. Today Phys. **5**, 1 (2018).

[47] L. C. Chen, H. Yu, H. J. Pang, B. B. Jiang, L. Su, X. Shi, L. D. Chen, and X. J. Chen, Pressure-induced enhancement of thermoelectric performance in palladium sulfide, Mater. Today Phys. **5**, 64 (2018).

[48] H. J. Pang, H. Yu, L. C. Chen, C. G. Fu, T. J. Zhu, and X. J. Chen, Pressure tuning of thermoelectric performance in FeNbSb, J. Alloys Compd. **805**, 1224 (2019).

[49] N. F. Mott and H. Jones, *The Theory of the Properties of Metals and Alloys* (Dover, New York, 1958).

[50] E. Maciá, May quasicrystals be good thermoelectric materials? Appl. Phys. Lett. **77**, 3045 (2000).

[51] J. R. Sootsman, D. Y. Chung, and M. G. Kanatzidis, New and old concepts in thermoelectric materials, Angew. Chem. Int. Ed. **48**, 8616 (2009).

[52] J. He and T. M. Tritt, Advances in thermoelectric materials research: Looking back and moving forward, Science **357**, eaak9997 (2017).

[53] I. M. Lifshitz, Anomalies of electron characteristics of a metal in the high pressure region, Sov. Phys. JETP **11**, 1130 (1960).

[54] H. J. Goldsmid and J. W. Sharp, Estimation of the thermal band gap of a semiconductor from Seebeck measurements, J. Electron. Mater. **28**, 869 (1999).

[55] E. D. Mun, S. L. Bud'ko, N. Ni, A. N. Thaler, and P. C. Canfield, Thermoelectric power and Hall coefficient measurements on $Ba(Fe_{1-x}T_x)_2As_2$ ($T$ = Co and Cu), Phys. Rev. B **80**, 054517 (2009).

[56] L. Fang, H. Q. Luo, P. Cheng, Z. S. Wang, Y. Jia, G. Mu, B. Shen, I. I. Mazin, L. Shan, C. Ren, and H.-H. Wen, Roles of multiband effects and electron-hole asymmetry in the superconductivity and normal-state properties of $Ba(Fe_{1-x}Co_x)_2As_2$, Phys. Rev. B **80**, 140508(R) (2009).

[57] F. Rullier-Albenque, D. Colson, A. Forget, and H. Alloul, Hall effect and resistivity study of the magnetic transition, carrier content, and Fermi-liquid behavior in $Ba(Fe_{1-x}Co_x)_2As_2$, Phys. Rev. Lett. **103**, 057001 (2009).

[58] C. Liu, T. Kondo, R. M. Fernandes, A. D. Palczewski, E. D. Mun, N. Ni, A. N. Thaler, A. Bostwick, E. Rotenberg, J. Schmalian, S. L. Bud'ko, P. C. Canfield, and A. Kaminski, Evidence for a Lifshitz transition in electron-doped iron arsenic superconductors at the onset of superconductivity, Nat. Phys. **6**, 419 (2010).

[59] S. V. Ovsyannikov and V. V. Shchennikov, High-pressure routes in the thermoelectricity or how one can improve a performance of thermoelectrics, Chem. Mater. **22**, 635 (2010).

[60] G. J. Snyder, A. Pereyra, and R. Gurunathan, Effective mass from Seebeck coefficient, Adv. Funct. Mater. **32**, 2112772 (2022).

[61] V. L. Kuznetsov, L. A. Kuznetsova, and D. M. Rowe, Effect of partial void filling on the transport properties of $Nd_xCo_4Sb_{12}$ skutterudites, J. Phys.: Condens. Matter **15**, 5035 (2003).

[62] Z. Y. Wang, J. Y. Xi, J. Y. Ning, K. Guo, B. Duan, J. Luo, G. J. Snyder, J. Yang, and W. Q. Zhang, Temperature-dependent band renormalization in $CoSb_3$ skutterudites due to Sb-ring-related vibrations, Chem. Mater. **33**, 1046 (2021).

[63] C. W. Chu, T. F. Smith, and W. E. Gardner, Study of Fermi-surface topology changes in rhenium and dilute Re solid solutions from $T_c$ measurements at high pressure, Phys. Rev. B **1**, 214 (1970).

[64] M. R. Norman, J. Lin, and A. J. Millis, Lifshitz transition in underdoped cuprates, Phys. Rev. B **81**, 180513(R) (2010).

[65] K. G. Sandeman, G. G. Lonzarich, and A. J. Schofield, Ferromagnetic superconductivity driven by changing Fermi surface topology, Phys. Rev. Lett. **90**, 167005 (2003).

[66] Y. Yamaji, T. Misawa, and M. Imada, Quantum and topological criticalities of Lifshitz transition in two-dimensional correlated electron systems, J. Phys. Soc. Jpn. **75**, 094719 (2006).

[67] E. A. Yelland, J. M. Barraclough, W. Wang, K. V. Kamenev, and A. D. Huxley, High-field superconductivity at an electronic topological transition in URhGe, Nat. Phys. **7**, 890 (2011).

[68] M. E. Barber, A. S. Gibbs, Y. Maeno, A. P. Mackenzie, and C. W. Hicks, Resistivity in the vicinity of a van Hove singularity: $Sr_2RuO_4$ under uniaxial pressure, Phys. Rev. Lett. **120**, 076602 (2018).

[69] Y. Okamoto, A. Nishio, and Z. Hiroi, Discontinuous Lifshitz transition achieved by band-filling control in $Na_xCoO_2$, Phys. Rev. B **81**, 121102(R) (2010).

[70] A. A. Abrikosov, *Fundamentals of the Theory of Metals* (North-Holland, Amsterdam, 1988).

[71] Y. M. Blanter, M. I. Kaganov, A. V. Pantsulaya, and A. A. Varlamov, The theory of electronic topological transitions, Phys. Rep. **245**, 159 (1994).

[72] N. N. Ablyazov, M. Y. Kuchiev, and M. E. Raikh, Topological transition and its connection with the conductivity and thermopower anomalies in two-dimensional systems, Phys. Rev. B **44**, 8802 (1991).

[73] N. B. Brandt, V. S. Egorov, M. Yu. Lavrenyuk, N. Ya. Minina, and A. M. Savin, Anomalies of thermoelectric power and of resistance in electronic topological transitions in bismuth and its alloys, Zh. Eksp. Teor. Fiz. **89**, 2257 (1985) [Sov. Phys. JETP **62**, 1303 (1985)].